GaSb molecular beam epitaxial growth on *p*-InP(001) and passivation with *in situ* deposited Al_2O_3 gate oxide

C. Merckling,[1,a] X. Sun,[2,3] A. Alian,[1,2] G. Brammertz,[1] V. V. Afanas'ev,[2] T. Y. Hoffmann,[1] M. Heyns,[1,2] M. Caymax,[1] and J. Dekoster[1]
[1]*Interuniversity Microelectronics Center (IMEC vzw), Kapeldreef 75, 3001, Leuven, Belgium*
[2]*Katholieke Universiteit Leuven, Celestijnelaan 200D, 3001, Leuven, Belgium*
[3]*Department of Electrical Engineering, Yale University, New Haven, Connecticut 06520-8284, USA*

(Received 8 December 2010; accepted 17 February 2011; published online 8 April 2011)

The integration of high carrier mobility materials into future CMOS generations is presently being studied in order to increase drive current capability and to decrease power consumption in future generation CMOS devices. If III–V materials are the candidates of choice for *n*-type channel devices, antimonide-based semiconductors present high hole mobility and could be used for *p*-type channel devices. In this work we first demonstrate the heteroepitaxy of fully relaxed GaSb epilayers on InP(001) substrates. In a second part, the properties of the Al_2O_3/GaSb interface have been studied by *in situ* deposition of an Al_2O_3 high-κ gate dielectric. The interface is abrupt without any substantial interfacial layer, and is characterized by high conduction and valence band offsets. Finally, MOS capacitors show well-behaved *C–V* with relatively low D_{it} along the bandgap, these results point out an efficient electrical passivation of the Al_2O_3/GaSb interface. © *2011 American Institute of Physics*. [doi:10.1063/1.3569618]

I. INTRODUCTION

Future complementary metal-oxide-semiconductor (CMOS) technologies will require the integration of higher carrier mobility materials to increase drive current capability.[1,2] One promising solution is to use a quantum-well field effect transistor (QWFET) device type combining a $Si_{(1-x)}Ge_x$ channel for *p*-QWFET with an $In_xGa_{(1-x)}As$ channel for *n*-QWFET, with $x > 0.5$.[3] However, in this scenario, several issues still need to be addressed, such as the cointegration on a common Si platform of IV–IV and III–V materials, which could lead to cross-contamination problems. This would justify the benefit of finding a suitable III–V material for the *p*-type channel in the potential view of a full III–V CMOS device. Even if all III–V materials present a hole mobility (for the bulk) lower than Ge, the possibilities of band engineering and the low hole effective mass in strained heterostructures make III–V *p* channels attractive. Antimonide-based III–V semiconductors present the unique property of owning both high electron (InSb) and high hole (GaSb) mobility, which triggered much of the interest in these III–Sb compounds for advanced CMOS. Actually, the integration of III–V's for MOSFET is still driven by n-MOS device realization and, except for recent results on an InSb-based quantum well device from Intel,[4] not many solutions for III–V *p*-MOSFET devices have been proposed at this time.

Interest in GaSb as the material of choice for *p*-MOS devices is mainly due to its attractive electrical properties, including its high hole mobility ($\mu_h \sim 1000\ cm^2\ V^{-1}\ s^{-1}$) and its narrow bandgap (~0.73 eV at 300 K), which is close to that of the perspective *n*-channel material like $In_{0.53}Ga_{0.47}As$ (~0.75 eV at 300 K) which is lattice matched to InP.[5] GaSb has a lattice constant of 6.09 Å and belongs together with AlSb and InAs binary compounds to the "6.1 Å" family.[6–8] These three III–V semiconductors form a lattice matched set around 6.1 Å and present a wide range of energy gaps from 0.36 eV for InAs to 1.61 eV for AlSb. The relatively large lattice parameter of GaSb makes the growth and the integration on standard surfaces difficult. But despite a very large lattice mismatch of 8%, the heteroepitaxy of high-quality GaSb layer on GaAs substrates has already been reported with[9,10] or without[11,12] the use of a buffer layer. It is possible to grow GaSb with low defect density on GaAs, due to the formation of a highly periodic array of 90° misfit dislocations at the GaSb/GaAs interface, which results in very low densities of threading dislocations.[13]

Regarding the III–V gate stack, for 40 years the interface and passivation between gate oxides and III–As compounds has been under extensive study, while only few studies on antimonides were reported. Recently, a study of Al_2O_3 deposited by atomic layer deposition (ALD) on HCl cleaned GaSb substrates showed that the III–V surface is very sensitive to the deposition temperature. The correlated electrical characterization has demonstrated low interface state trap density (D_{it}) values close to the valence band edge despite the presence of Sb-oxides at the interface.[14,15]

In order to avoid any undesirable interfacial layer formation by oxidation of GaSb, molecular beam epitaxy (MBE) would be an attractive technique, due to its potential to control *in situ* the III–V surface, the high-κ dielectric deposition, and the interface between both materials at the atomic scale.[16,17] In this context, we report first on a MBE study of the heteroepitaxy of *p*-type doped GaSb on InP(001) substrates. The structural quality of the growth was examined using high resolution x-ray diffraction, transmission electron microscopy (TEM), and atomic force microscopy (AFM). After the growth, the molecular beam deposition of an Al_2O_3

[a]Author to whom correspondence should be addressed. Electronic mail: clement.merckling@imec.be.

high-κ gate oxide layer is performed in a virtual *in situ* approach (by the use of a protective As-cap layer) on the reconstructed GaSb(001) surface. Reflection high-energy electron diffraction (RHEED) and x-ray photoelectron spectroscopy (XPS) were used to investigate the structural and chemical properties of the Al_2O_3/GaSb gate stack. Internal photoemission (IPE) and photoconductivity (PC) spectroscopy have been applied to extract the Al_2O_3/GaSb interface band offsets. Finally, electrical characterization like capacitance-voltage ($C-V$) and conductance–voltage (G–V) measurements[18] done at 300 K [room temperature (RT)] and 77 K [low temperature (LT)] are employed to extract defect density close the valence band edge and midgap region in order to estimate the passivation efficiency at the Al_2O_3/GaSb interface.

II. EXPERIMENTAL

The growth of Al_2O_3/GaSb/InP(001) heterostructures has been carried out in two different MBE clusters. First, the III–V layers were grown in a 2 in. Riber 2300 system. The GaSb layers were grown on 2 in. *p*-type InP(001) "epiready" wafers (obtained from AXT Inc.). Standard effusion cells are used for Ga and Sb metals while a valved As cracker source is used for the InP surface preparation. After growth, to prevent the GaSb surface from oxidation, an amorphous arsenic cap layer ($\sim$1 μm thick) was deposited at RT on top of the GaSb thin film. Then, the samples are introduced in a Riber 200 mm molecular beam epitaxy cluster. First, the As cap is removed in the preclean chamber and monitored by RHEED. The complete desorption of the protective As layer is obtained at 400 °C with the appearance of a streak (1×3) GaSb(001) reconstructed surface.[19] Finally, the sample was introduced into the oxide chamber to perform the molecular beam deposition of the high-κ dielectric. The Al_2O_3 thin films were grown by codeposition of aluminum with atomic oxygen at an overall pressure of 3×10^{-6} Torr. During the deposition, the substrate temperature was around $T_D = 50$ °C in order to obtain an amorphous layer. MOS capacitors were made by means of 150 nm Ni metal dots deposited through a shadow mask. The back-side Ohmic contact was formed using a composite stack of 30 nm of Au followed by 70 nm of AuZn for *p*-type InP substrates. After metal deposition, samples are annealed at 300 °C for 30 s in a forming gas (N_2/H_2) environment.

III. RESULTS

A. Epitaxial growth of GaSb on InP: Physical characterizations

We start with the investigation of the heteroepitaxial growth of GaSb on InP(001) substrate. The native oxide of the InP(001) surface is thermally desorbed under group-V element overpressure in order to prevent thermal desorption of the phosphorus which would destroy the wafer surface. Therefore, the native oxide desorption is carried out under arsenic overpressure. The de-oxidation process developed to prepare a clean "oxygen-free" InP surface is monitored in real time by RHEED analysis. After introduction in the MBE chamber, a clean (2×1) surface reconstruction is observed by RHEED at 300 °C. To completely remove the native oxide, the substrate is heated, under an arsenic overpressure of $P(As_4) = 1 \times 10^{-5}$ Torr, until the apparition of a $(\times 4)$ reconstruction along the [110] azimuth is observed. This RHEED transition from the initial (2×1) to a (4×1) surface reconstruction takes place at 565 °C and indicates the total desorption of the InP native oxide.[20] In order to avoid damage to the III–V surface, the substrate temperature is immediately reduced to the GaSb growth temperature after the apparition of the $(\times 4)$ reconstruction along the [110] direction. At a substrate temperature of 400 °C, the As is closed for a few minutes before opening the Sb shutter. The *p*-GaSb film is deposited by a two-step growth. First, a low temperature buffer is grown at 430 °C with a low growth rate ($(v_G)_{LT} = 0.15$ ML s^{-1}). After 30 nm of growth, the substrate temperature is gradually increased by 100 °C. The main layer is grown at 530 °C, at a growth rate of 0.5 ML s^{-1} and Si doped at 3×10^{18} cm^{-3} (Si is acceptor for GaSb compound[21]). During growth, the GaSb epilayer presents a streak (1×3) Sb-stabilized surface reconstruction. At the end of the growth, the substrate temperature is reduced under antimony overpressure and stopped below 350 °C, leading to a GaSb(001)–(1×5) Sb-rich reconstructed surface. Finally, a 1 μm As cap was deposited to protect the GaSb surface during the transfer from the III–V to the oxide MBE tool.

In order to study the structural quality of the GaSb/InP heterostructure, a dark-field cross-sectional transmission electron microscopy (TEM) image taken along $\langle 110 \rangle_{InP}$ is shown in Fig. 1(a). First, the GaSb film appears to be completely relaxed on InP substrate. This TEM image attests of the good crystalline quality of the layer: the thin film presents a uniform thickness of $\sim$1.1 μm with a smooth GaSb top surface and the GaSb/InP(001) interface is sharp and continuous without pinholes. Surprisingly, despite the large mismatch of 3.8% between both lattices the GaSb layer presents a very low defect density without obvious threading dislocations. Only bright (in DF-TEM, dark in TEM) round features are visible in the GaSb layer. These artifacts are coming from the

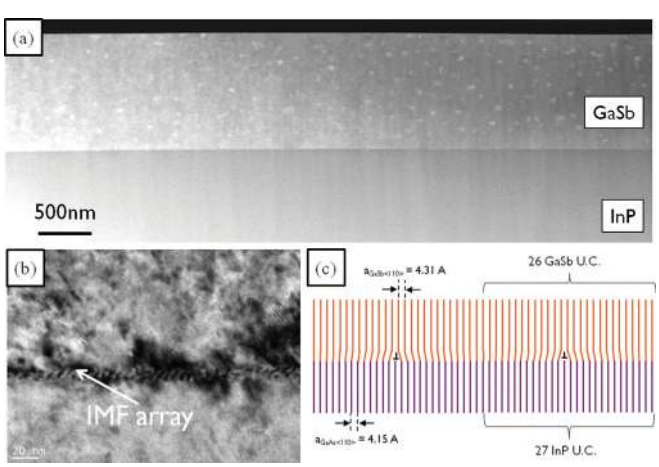

FIG. 1. (Color online) (a) Dark field TEM cross-sectional image of the GaSb/InP(001) heterostructure taken by selecting the 004 reflection of GaSb. (b) High resolution TEM cross-sectional zoom of the interface showing the presence of interfacial misfit network. (c) Illustration of the coincidence epitaxial relationship between both lattices.

sample preparation with the interaction between the Ga beam of the Focused Ion Beam (FIB) and the GaSb layer.[22] In fact, like on GaAs,[23] the relaxation process takes place through the formation of an interfacial misfit dislocation network as shown in Fig. 1(b). This regular interfacial dislocation array leads to the complete relaxation of GaSb in only a few nanometers of growth. The average distance between two misfit dislocations is around 11 nm, which would then correspond to the perfect coincidence of 26 GaSb unit cells with 27 unit cells of InP substrate as sketched in Fig. 1(c), which corresponds to the 3.8% lattice mismatch.

In order to investigate the crystalline quality of the GaSb/InP heterostructure we performed a reciprocal space mapping around the (115) Bragg reflections. The asymmetric (115) cartography of a 1.1-μm-thick GaSb layer on InP(001) sample, shown in Fig. 2, provides reciprocal lattice vector components related directly to both the in-plane and out-of-plane lattice parameters. The thin and intense peak centered at (0.2396 $Å^{-1}$; 0.8442 $Å^{-1}$) corresponds to the (115) Bragg reflection of the InP(001) substrate while the broader peak located at (0.2350 $Å^{-1}$; 0.8292 $Å^{-1}$) corresponds to the diffraction of the (115) planes of the GaSb film. This mapping confirms the high crystallinity of the GaSb epilayer and indicates that the GaSb is almost completely relaxed. Effectively, the in-plane and out of plane lattice parameter of GaSb extracted from these measurements are respectively $(a_{\parallel})_{GaSb} = 0.60855 \pm 0.001$ nm and $(a_{\perp})_{GaSb} = 0.6085 \pm 0.001$ nm corresponding to a relaxation of more than 95% in both directions. The (115) GaSb Bragg reflection on the reciprocal space map presents a particular shape which evidences an anisotropic elongation in the orthogonal directions. We attribute this mosaic aspect to the presence of defects generated by the interfacial misfit dislocation network formation and relaxation of the GaSb film during the early stage of the growth on the InP substrate.

In order to study the surface morphology, *ex situ* AFM measurements in tapping mode were carried out. Figure 3(a) shows the topographic image of the GaSb(001) epilayer. The GaSb surface is flat and exhibits the clear formation of a uniform step-and-terrace pattern. Moreover, no cross hatch, corresponding to the presence of a threading dislocation network in a semiconductor, has been detected at the surface. But the topographic AFM scan clearly exhibits the emergence of isolated spiral dislocations on the top surface.[11] The step height is about 0.3 nm [as seen on the profile in Fig. 3(b)], which corresponds to one GaSb monolayer. The average rms roughness and peak-to-valley values are 0.29 and 3 nm, respectively, over a 1 μm $\times$ 1 μm scan area. Finally, atomic force microscopy shows a 2D film with large scale roughness and demonstrates that the GaSb growth occurred essentially by step-flow mode and reveals the presence of emerging dislocations in the layer, which was very difficult to show by TEM analysis.

B. Molecular beam deposition of Al_2O_3 on GaSb(001)

The As-decapping step is done in a preclean chamber and RHEED has been used to monitor in real time the evolution of the surface. A thermal anneal in ultrahigh vacuum (UHV) up to 400 °C allows the complete desorption of the protective As-cap layer. This is confirmed by the recovery of a streak

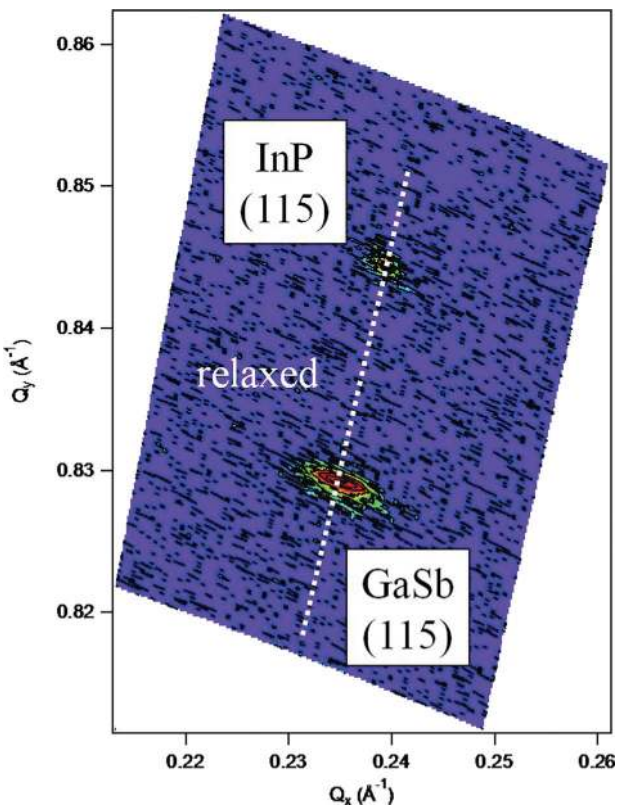

FIG. 2. (Color online) Reciprocal space map around the (1 1 5) Bragg reflection of the InP substrate and the GaSb epilayer.

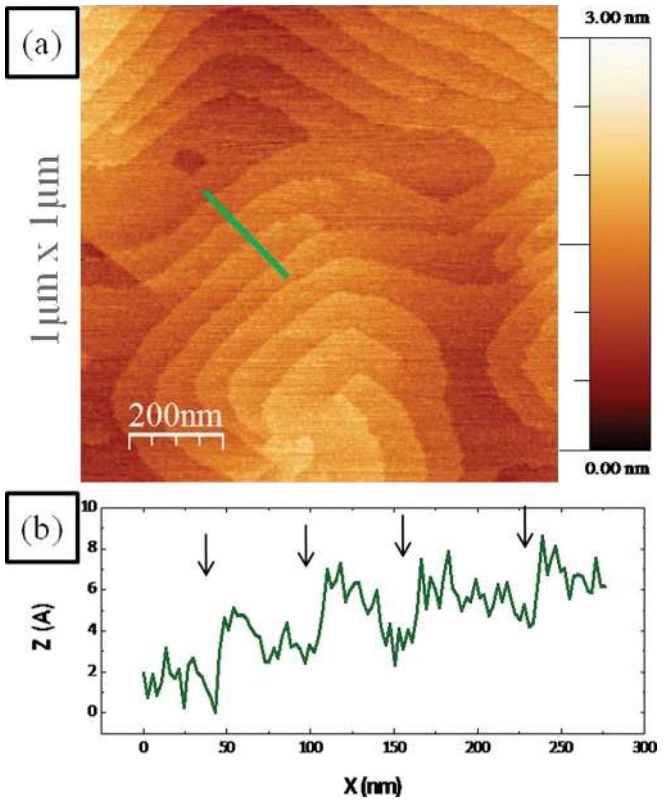

FIG. 3. (Color online) (a) AFM topographic image (1 μm $\times$ 1 μm) of the GaSb layer surface grown on InP(001) substrate. The surface is showing a clear steps-and-terraces morphology with a step height of one monolayer as shown on the Z profile (b).

"Sb-stabilized" (1×3) surface reconstruction[24] as shown on the RHEED diffraction patterns in Fig. 4(a). This (1×3) reconstructed surface, as illustrated in Fig. 4(b), corresponds to the formation of parallel Sb dimer rows on the surface.[25]

A 2-nm-thick Al_2O_3/GaSb–(1×3)/InP(001) stack was realized in order to investigate by means of XPS analysis the chemical properties and interface quality after *in situ* oxide deposition (Fig. 5). XPS spectra were recorded at a detection angle of 21.875° with respect to the normal of the surface in order to increase the sensitivity for the Al_2O_3/GaSb interface. In Fig. 5(a) the peak centered at 18.9 eV corresponds to the Ga *3d* core level. The peak is composed of a single doublet ($3d_{3/2}$ and $3d_{5/2}$ components), indicating there is only one chemical configuration present of Ga bonded to Sb, no oxidation of the gallium peak was observed. The Sb $3d_{3/2}$ core level spectrum, shown in Fig. 5(b), is centered at 537.1 eV and presents one doublet with a Sb $3d_{5/3}$ peak at 527.8 eV. In the same region, in between both Sb *3d* peaks, we can notice the presence of the O 1*s* core level at 531.2 eV from the thin Al_2O_3 gate oxide. The Sb $3d_{3/2}$ peak displayed no features at higher binding energy, which reveals no presence of Sb_2O_3 or Sb suboxides at the Al_2O_3/GaSb interface. The sharpness of the oxide/III–V interface demonstrates the perfect control during the initial stage of the Al_2O_3 molecular beam deposition to prevent undesirable interfacial layer formation.

In order to study the structural quality of the Al_2O_3/GaSb interface, a high resolution cross-sectional transmission electron microscopy (HRTEM) image taken along $\langle 110 \rangle_{InP}$ is shown in Fig. 6. The Al_2O_3 thin film presents a uniform thickness of 5 ± 0.2 nm and a flat surface. The Al_2O_3/GaSb interface is sharp at the atomic-scale and continuous. The Al_2O_3 thin film is completely amorphous, it does not present any crystallites in the layer and the HRTEM image does not exhibit any thin interfacial layer. The TEM picture evidences the good homogeneity of the stack, the absence of interfacial defects (like pinholes, etch, etc.) on the GaSb surface, which could occur during the first step of the oxide deposition, but confirms the presence of threading dislocations visible in the GaSb epilayer.

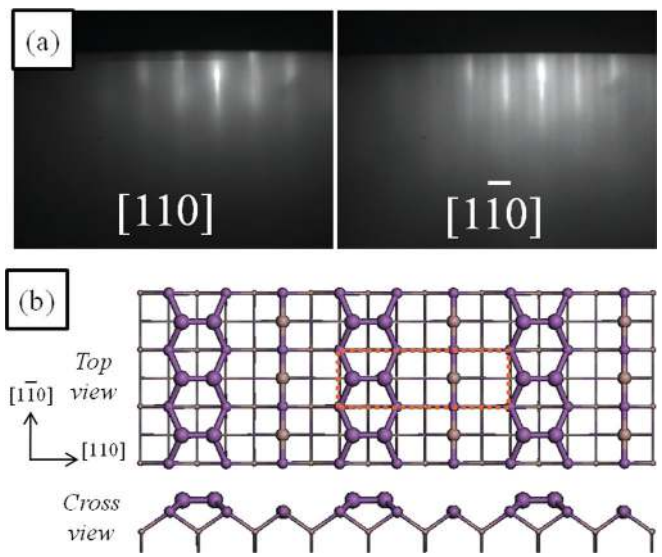

FIG. 4. (Color online) (a) RHEED patterns recorded along the [110] and [1 $\bar{1}$ 0] azimuths of the reconstructed GaSb(001) surface after As-decapping. The III–V surface is presenting a (1×3) periodicity, corresponding to a Sb-stabilized surface reconstruction, as illustrated in (b).

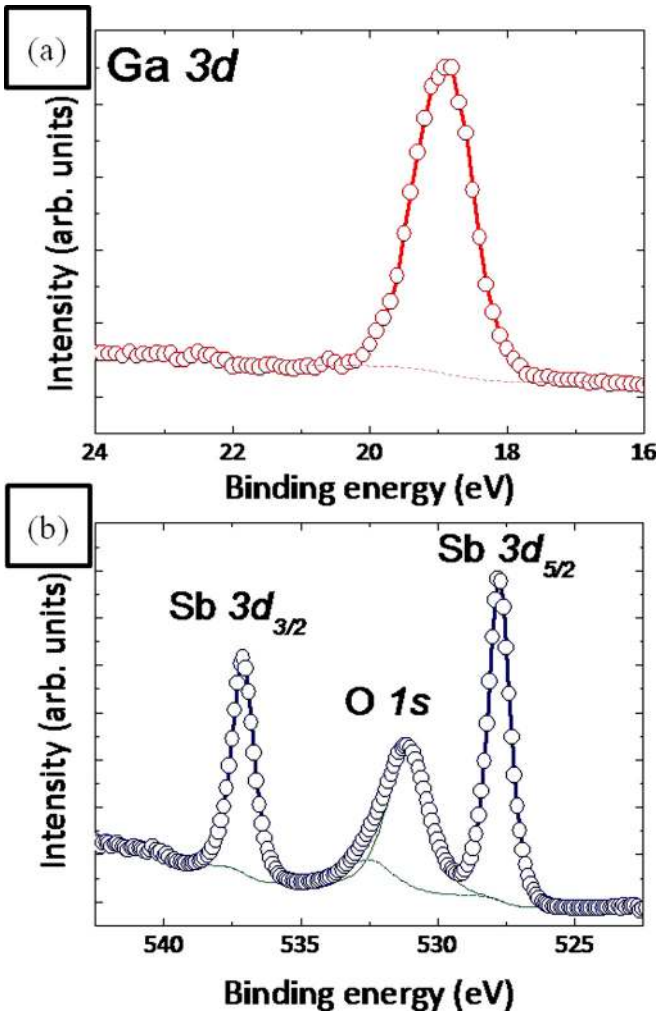

FIG. 5. (Color online) XPS Ga 3*d* (a) and Sb 3*d* (b) core level spectra of a 1-nm-thick Al_2O_3/GaSb/InP(001) heterostructure. The interface is free of interfacial suboxides.

C. Electrical characterization of Al_2O_3/GaSb interface

The absence of a substantial interlayer associated with GaSb surface oxidation is independently affirmed by the results of IPE/PC experiments conducted in MOS capacitors prepared

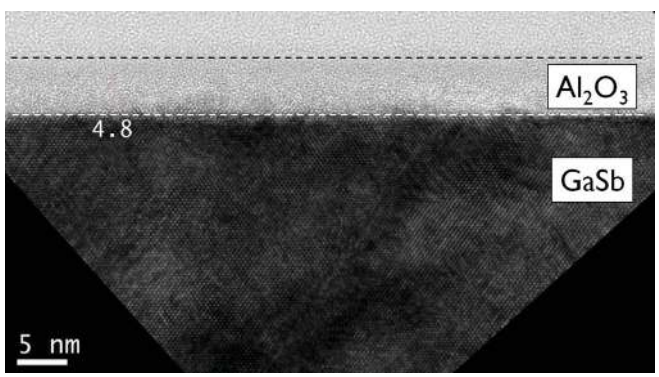

FIG. 6. (Color online) TEM picture of an Al_2O_3/GaSb/InP(001) heterostructure showing a very sharp oxide/III–V interface.

by evaporation of semitransparent (15-nm-thick) Au or Al electrodes on top of 10-nm-thick alumina layer. The IPE/PC spectra were measured at room temperature in the photon energy range 2–6.5 eV with constant spectral resolution of 2 nm with positive (+1 V) or negative (−1 V) bias applied to the top metal electrode. Then the quantum yield (Y), defined as the photocurrent normalized to the incident photon flux, was analyzed as a function of photon energy to determine energy thresholds of IPE from GaSb and metal electrodes and the onset of PC in the insulating layer.[26,27] The overview logarithmic plots of the quantum yield are shown in Fig. 7(a) for Al- (circles) and Au-gated (squares) samples as measured under positive (open symbols) and negative (closed symbols) bias on the metal electrodes. To isolate electron transitions associated with the oxide PC, we have looked for the equal spectral threshold energies in both Al- and Au-gated samples at two bias polarities. Assuming that in the amorphous oxide band-to-band electron transitions require no momentum conservation, the spectral thresholds were determined from the $Y^{1/2}$–$h\nu$ plots as shown in Fig. 7(b).[26] At high photon energy ($h\nu > 6$ eV) the observed increase in the yield can be associated with excitation of intrinsic PC in a-Al_2O_3. Reassuring this identification, the corresponding threshold energy of $E_g(Al_2O_3) = 6.1 \pm 0.1$ eV appears to be close to the value found earlier in alumina layers grown using atomic layer deposition technique.[28] One also can find there the second common spectral threshold at 4.1 ± 0.1 eV, which is close to the bandgap of Ga_2O_3 layers grown by the molecular beam deposition on GaAs(001).[29] As Al_2O_3 remains transparent in the spectral range $4 < h\nu < 6$ eV in which GaO_x PC is detected, from the ratio between the initial slopes of the PC spectra of Al_2O_3 and GaO_x one can evaluate the relative content of the latter phase to be below 1%. For the 10 nm thickness of the Al_2O_3 layer this would correspond to 0.1 nm upper limit of the GaO_x equivalent thickness, i.e., less than 1 monolayer of Ga_2O_3 may be present at the interface, which is consistent with the above-discussed cross-sectional TEM analysis and XPS.

In the low photon energy range ($h\nu < 6$ eV) the spectra measured under positive bias are clearly different from those obtained at negative bias indicating that IPE from electrodes of MOS capacitor becomes the source of photocurrent. The positive bias spectra exhibit modulation at the photon energies corresponding to direct optical transitions in GaSb at $E_0' = 3.3$ eV ($\Gamma_8^v - \Gamma_7^c$ transition) and $E_2 = 4.1$ eV ($X_5^v - X_1^c$ and Σ^v–Σ^c transitions)[30] indicating electron IPE from the GaSb valence band (VB) to the conduction band (CB) of Al_2O_3 as the dominant signal. The corresponding spectral threshold (Φ_e) was found from the $Y^{1/3}$–$h\nu$ plot[31] to be 3.0 eV for both Al- and Au-gated samples as exemplified in the insert in Fig. 7(b). As the field-induced interface barrier lowering (the Schottky effect) in the case of Al_2O_3 insulator does not exceed 0.1 eV in the electric field with a strength below 1 MV/cm,[27] the indicated threshold of $\Phi_e = 3.0$ eV allows one to estimate the CB and VB offsets at the Al_2O_3/GaSb interface as 2.3 ± 0.1 and 3.0 ± 0.1 eV, respectively. These offsets are larger than those at the Si(001)/Al_2O_3 interface[27] suggesting good insulating properties of the Al_2O_3/GaSb interface. The additional low-energy "tail" in the case of Al gate is associated with the strong additional electric field

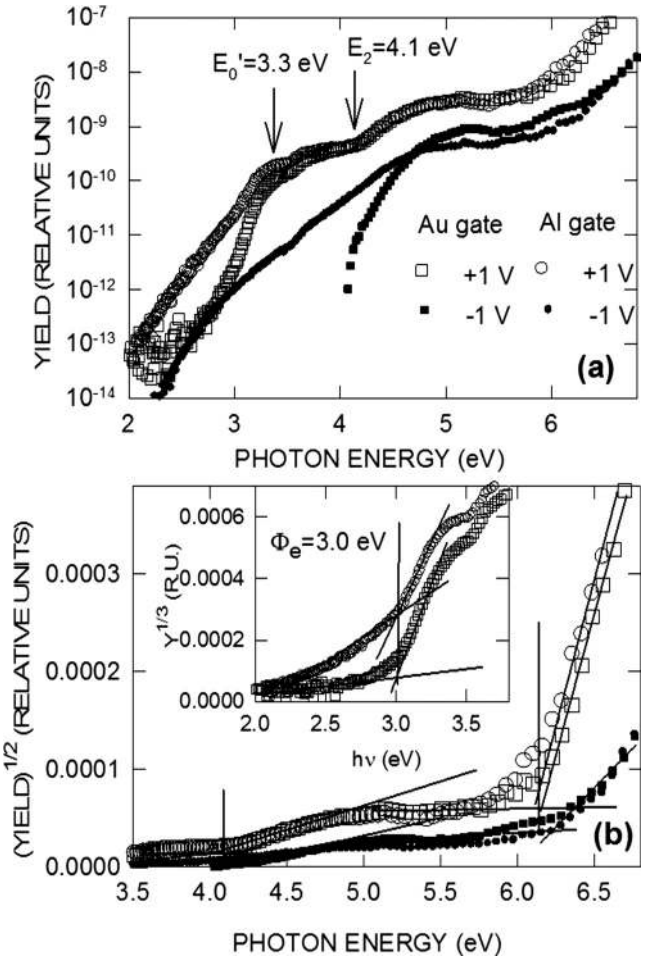

FIG. 7. (a) IPE/PC yield as a function of photon energy in p-type GaSb(001)/Al_2O_3 MOS capacitors with Al (circles) or Au (squares) electrodes measured under positive (open symbols) and negative (closed symbols) voltage of 1 V applied to the metal. Vertical arrows indicate the energies of direct optical transitions in GaSb crystal. (b) Determination of the PC thresholds using $Y^{1/2}$–$h\nu$ plots from the spectra shown in panel (a). The insert illustrates determination of the energy threshold of electron IPE from the GaSb VB to the Al_2O_3 CB using the $Y^{1/3}$–$h\nu$ plot. Vertical lines mark the inferred thresholds.

caused by the built-in voltage associated with metal-semiconductor workfunction difference. The field penetration into heavily p-doped GaSb photoemitter leads to the IPE of electrons excited in the bulk of the semiconductor by low-energy photons and gaining additional energy in the space charge layer of GaSb(p^+) (see, e.g., Fig. 2.1.3 in Ref. 27).

Finally, to assess the passivation of the Al_2O_3/p-GaSb interface, electrical characterization including C–V measurements, simulation, and ac conductance[32] was performed on Ni/9 nm-Al_2O_3/p-GaSb (3×10^{18} cm^{-3} Si-doped)/p-InP (001) MOS stacks after PDA/PMA (FGA 450 °C 5 min/280 °C 10 min). Figure 8 presents the C–V characteristics measured at 300 K with gate voltage swept from inversion to accumulation at multiple frequencies ranging from 100 Hz to 1 MHz. The C–V curves are well behaved with clearly articulated accumulation, depletion, and inversion regions. The C–V curves at 300 K show relatively small frequency dispersion in accumulation (~6% from 100 Hz to 1 MHz) and frequency dependent weak inversion response due to the narrow bandgap of GaSb (0.73 eV). At 300 K, even with higher doping the C_{min} ditch of multifrequency C–V is deeper than the recently published

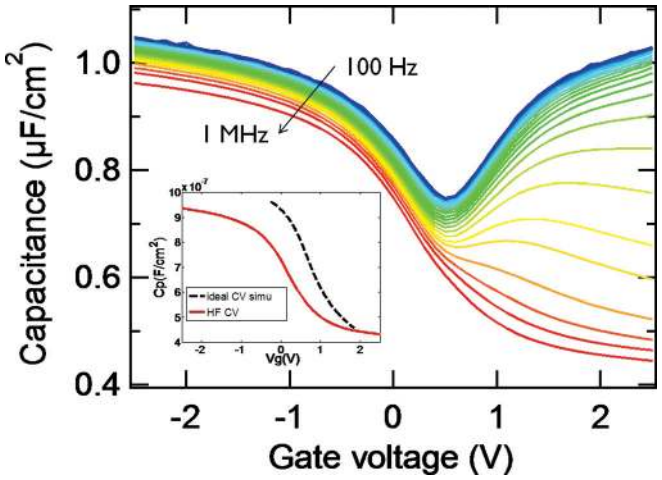

FIG. 8. (Color online) Room temperature (300 K) *C–V* characteristics of Al_2O_3/GaSb(Si)/InP MOS capacitors. Difference between the ideal and measured high frequency curves are shown in the inset.

HCl treated PEALD Al_2O_3/GaSb,[14] indicating a smaller D_{it} near midgap. The D_{it} distribution near midgap is evaluated as $\sim 2 \times 10^{12}$ eV^{-1} cm^{-2} using the Terman method (the inset of Figs. 8 and 9).

To accurately probe the D_{it} near the valance band edge, the Al_2O_3/*p*-GaSb interface was characterized by the ac conductance method at low temperatures from 77 to 200 K.[32] Beyond 200 K, the conductance of weak inversion will contribute to the measured signal masking the traps response. At 77 K, the *C–V* dispersion is reduced to 2% indicating an average low D_{it} near the valance band edge. The conductance contour for various temperatures is shown in Fig. 9(a). The curves in the contour label the conductance peak movement with respect to gate bias. The *y* axis $\ln(\omega)$ is proportional to Fermi level position, the so-called Fermi level trace.[33] The trace shows no sign of Fermi level pinning from deep depletion to weak inversion in the bandgap. Figure 9(b) summarizes the D_{it} distribution with respect to the energy in lower half of the bandgap extracted by ac conductance and Terman method. The D_{it} near the valance band edge is seen to be of the order of low 10^{12} eV^{-1} cm^{-2} and becomes even lower toward the midgap. The half of "U" shape D_{it} profile agrees with the Spicer's model on GaSb.[34] Such a D_{it} profile is promising for the *p*-channel transistor applications and suggests possibility to attain a low subthreshold swing and smooth inversion.

IV. DISCUSSION

In the first part of this paper, we studied the molecular epitaxial growth of GaSb on InP(001) substrates. Physical characterization demonstrates that it is possible to grow a relatively high quality fully relaxed GaSb layer despite a ~4% lattice mismatch between both III–V semiconductors. In fact, the plastic relaxation happened at the early stage of the GaSb heteroepitaxy. As observed by high resolution TEM, the large lattice mismatch with the InP substrate is accommodated by periodic arrays of misfit (or Lomer-type) dislocations that are confined at the interface. The propagation of dislocations through the epilayer is extremely limited. It was possible to reveal the presence of emerging dislocations in the GaSb layer by AFM,

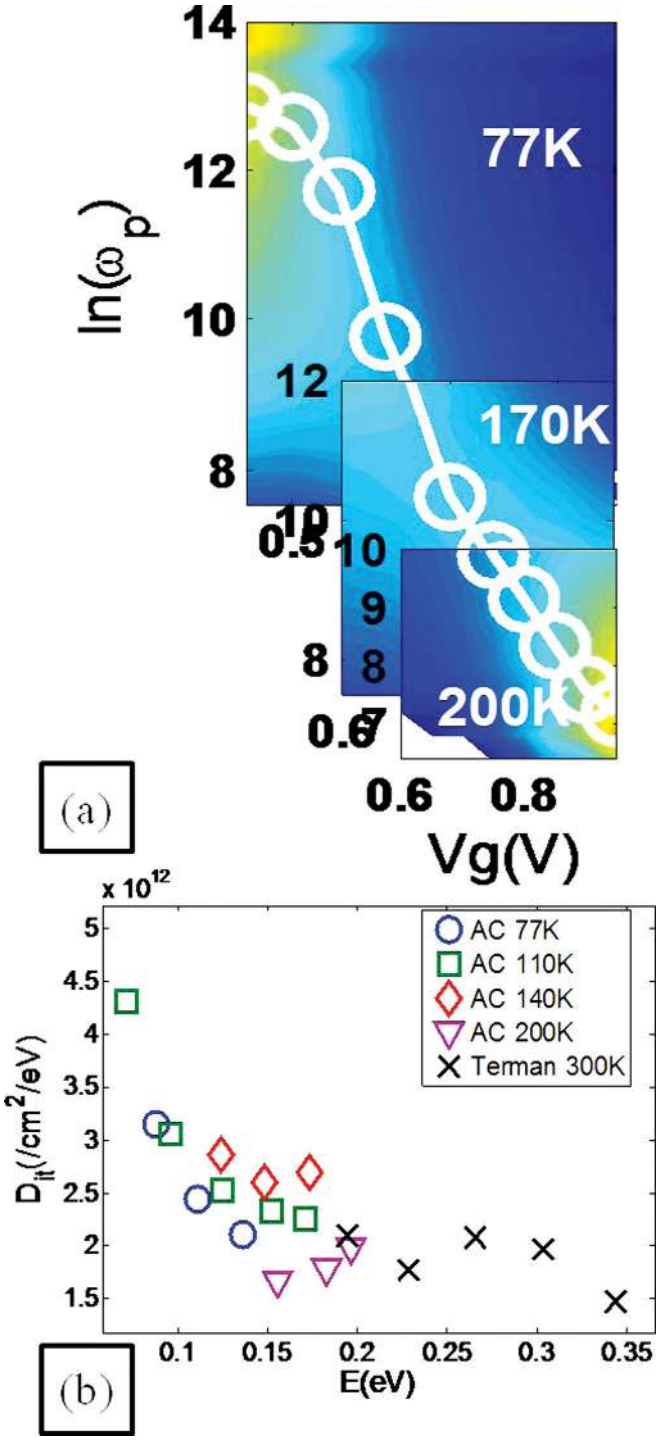

FIG. 9. (Color online) (a) Conductance mapping revealing the Fermi level trace from GaSb midgap to the valence band edge. (b) D_{it} distribution as a function of the energy above E_V for Al_2O_3/*p*-GaSb MOS capacitor. D_{it}'s are extracted by conductance method with varying *C–V* measurement temperatures near valence band and Terman method around midgap.

while it was impossible by standard TEM analyses. A possibility to improve the GaSb buffer layer quality would be to make use of a mixed GaAlSb initiation layer grown on InP. But despite the presence of crystalline defects in low density in the GaSb film, meaning that there is room for structural quality enhancement, these layers are fine to investigate the electrical properties of the high-κ oxide/GaSb interface. This has been studied in the second part of the manuscript.

Most of the III–V semiconductor surfaces are very sensitive to oxygen compounds that will generate the formation of native oxide. This undesirable interlayer will contribute aggressively to the high density of surface states within the energy bandgap, resulting in Fermi level pinning (FLP) which disturbs the basic III-V MOSFET operation.[35] For these reasons we studied the *in situ* passivation by amorphous Al_2O_3 oxide and we demonstrated here the efficiency of an As-cap layer on the III–Sb surface to protect and recover the original Sb-stabilized (1×3) surface reconstruction. We focused then on a "smooth" deposition of the high-κ oxide to avoid the overoxidation of the GaSb layer during the initial stage of the growth. We obtained a very sharp and stable Al_2O_3/GaSb interface. Effectively, it was not possible to detect by XPS analyses any presence of interfacial oxide, while IPE/PC measurements could reveal only a weak GaO_x signal (lower than 1% from the GaO_x/Al_2O_3 PC yield ratio) at the interface. As no Sb suboxide has been detected by XPS or IPE/PC investigations it means that the connection of the oxide network takes place essentially via Ga–O–Al interfacial bonds. The corresponding *C–V/G–V* characterizations on the *p*-type GaSb layer demonstrated well behaved *C–V*'s at room and low temperatures, associated with a good Fermi level modulation close to the valence band edge. The behavior of the Al_2O_3/GaSb interface brings some elements for the realization of a *p*-QWFET quantum well device. In particular, GaSb layer could be used as an efficient passivation layer with low D_{it} in the device operation region.

V. CONCLUSIONS

In summary, we have reported here the heteroepitaxy of GaSb directly on InP(001) substrates using solid source molecular beam epitaxy. High quality and relaxed GaSb layers have been obtained due to the misfit dislocation network formed at the interface. Then both structural and electrical investigations of the molecular beam passivation of GaSb by amorphous alumina have been realized. A well-controlled *in situ* surface preparation of GaSb and molecular beam deposition of Al_2O_3 result in an efficient passivation with abrupt oxide/semiconductor interface, large interface band offsets, low D_{it} values, and thermodynamically stable structures. Further investigations are required to fully understand the initial growth mechanism. The electrical passivation of GaSb will also be further addressed and optimized by the use of chalcogen surface treatments. Finally, the high morphological quality of the relaxed GaSb layers confirms the possibility of using twin-free GaSb epitaxially grown on InP as pseudosubstrate for the realization of "6.1 family"-based devices.

ACKNOWLEDGMENTS

This work is part of the IMEC Industrial Affiliation Program and is supported by the European Commission's project FP7-ICT-DUALLOGIC no. 214579, "Dual-Channel CMOS for (sub)-22nm High Performance Logic." The authors would like to thank Th. Conard and A. Franquet for XPS characterizations, F. Paola and H. Bender for TEM analyses, and H. Costermans for the support of the MBE tool.

[1] M. Heyns, M. Meuris, and M. Caymax, ECS Trans. **3**, 511 (2006).
[2] See, e. g., *Advanced Gate Stacks for High Mobility Semiconductors*, edited by A. Dimoulas, E. Gusev, P. C. McIntyre, and M. Heyns (Springer, Berlin, 2007).
[3] M. Passlack, K. Rajagopalan, J. Abrokwah, and R. Droopad, IEEE Trans. Electron Devices **53**, 2454 (2006).
[4] M. Radosavljevic, T. Ashley, A. Andreev, S. D. Coomber, G. Dewey, M. T. Emeny, M. Fearn, D. G. Hayes, K. P. Hilton, M. K. Hudait, R. Jefferies, T. Martin, R. Pillarisetty, W. Rachmady, T. Rakshit, S. J. Smith, M. J. Uren, D. J. Wallis, P. J. Wilding, and R. Chau, IEDM Tech. Dig., pp.727 (2008).
[5] See http://www.ioffe.ru/SVA/NSM/
[6] L. L Chang and L. Esaki, Surf. Sci. **98**, 70 (1980).
[7] G. Tuttle, H. Kroemer, and J. H. Emglish, J. Appl. Phys. **65**, 5239 (1989).
[8] H. Kroemer, Physica E. **20**, 196 (2004).
[9] M. Thomas, H.-R. Blank, K. C. Wong, and H. Kroemer, J. Cryst. Growth **175/176**, 894 (1997).
[10] H. S. Kim, Y. K. Noh, M. D. Kim, Y. J. Kwon, J. E. Oh, Y. H. Kim, J. Y. Lee, S. G. Kim, and K. S. Chung, J. Cryst. Growth. **301–302**, 230 (2007).
[11] S. H. Huang, G. Balakrishnan, A. Khoshakhlagh, A. Jallipalli, L. R. Dawson, and D. L. Huffaker, Appl. Phys. Lett. **88**, 131911 (2006).
[12] R. Hao, Y. Hu, Z. Zhou, Z. Ren, H. Ni, Z. He, and Z. Niu, J. Phys. D: Appl. Phys. **40**, 1080 (2007).
[13] S. H. Huang, G. Balakrishnan, M. Mehta, A. Khoshakhlagh, L. R. Dawson, D. L. Huffaker, and P. Li, Appl. Phys. Lett. **90**, 161902 (2007).
[14] A. Ali, H. S. Madan, A. P. Kirk, D. A. Zhao, D. A. Mourey, M. K. Hudait, R. M. Wallace, T. N. Jackson, B. R. Bennett, J. B. Boos, and S. Datta, Appl. Phys. Lett. **97**, 143502 (2010).
[15] I. Geppert, M. Eizenberg, A. Ali, and S. Datta, Appl. Phys. Lett. **97**, 162109 (2010).
[16] Y. C. Chang, C. Merckling, J. Penaud, C. Y. Lu, W.-E. Wang, J. Dekoster, M. Meuris, M. Caymax, M. Heyns, J. Kwo, and M. Hong, Appl. Phys. Lett. **97**, 112901 (2010).
[17] C. Merckling, J. Penaud, D. Kohen, F. Bellenger, A. Alian, G. Brammertz, M. El-Kazzi, M. Houssa, J. Dekoster, M. Caymax, M. Meuris, and M. M. Heyns, Microelectron. Eng. **86**, 1592 (2009).
[18] G. Brammertz, H. C. Lin, K. Martens, A. Alian, C. Merckling, J. Penaud, D. Kohen, W.-E Wang, S. Sioncke, A. Delabie, M. Meuris, M. Caymax, and M. Heyns, ECS Trans. **19**, 375 (2009).
[19] Q.-K. Xue, T. Hashizume, and T. Sakurai, Prog. Surf. Sci. **56**, 1 (1997).
[20] M. Gendry, V. Drouot, C. Santinelli, G. Hollinger, C. Miossi, and M. Pitaval, J. Vac. Sci. Technol. B. **10**, 1829 (1992).
[21] T. M. Rossi, D. A. Collins, D. H. Chow, and T. C. McGill, Appl. Phys. Lett. **57**, 2256 (1990).
[22] A. Lugstein, C. Schoendorfer, M. Weil, C. Tomastik, A. Jauss, and E. Bertagnolli, Nucl. Instrum. Methods Phys.Res.B **255**, 309 (2007).
[23] A. Jallipalli, G. Balakrishnan, S. H. Huang, A. Khoshakhlagh, L. R. Dawson, and D. L. Huffaker, J. Cryst. Growth. **303**, 449 (2007).
[24] A. S. Bracker, M. J. Yang, B. R. Bennett, J. C. Culbertson, and W. J. Moore, J. Cryst. Growth. **220**, 384 (2000).
[25] M. T Sieger, T. Miller, and T.-C. Chiang, Phys. Rev. B **52**, 8256 (1995).
[26] V. V. Afanas'ev and A. Stesmans, J. Appl. Phys. **102**, 081301 (2007).
[27] V. V. Afanas'ev, *Internal Photoemission Spectroscopy: Principles and Applications* (Elsevier, Amsterdam, 2008).
[28] V. V. Afanas'ev, M. Houssa, A. Stesmans, and M. M. Heyns, J. Appl. Phys. **91**, 3079 (2002).
[29] V. V. Afanas'ev, A. Stesmans, R. Droopad, M. Passlack, L. F. Edge, and D. G. Schlom, Appl. Phys. Lett. **89**, 092103 (2006).
[30] See, e. g., V. I. Gavrilenko, A. M. Grekhov, D. V. Korbutyak, and V. G. Litovchenko, *Optical Properties of Semiconductors* (Naukova Dumka, Kiev, 1987).
[31] R. J. Powell, J. Appl. Phys. **41**, 2424 (1970).
[32] E. H. Nicollian and J. R. Brews, *MOS Physics and Technology* (Wiley, New York, 1982).
[33] H. C. Lin, G. Brammertz, K. Martens, G. de Valicourt, L. Negre, W. E. Wang, W. Tsai, M. Meuris, and M. Heyns, Appl. Phys. Lett. **94**, 153508 (2009).
[34] W. E. Spicer, P. W. Chye, P. R. Skeath, C. Y. Su, and I. Lindau, J. Vac. Sci. Technol. **16**, 1422 (1979).
[35] G. Brammertz, H. C. Lin, K. Martens, D. Mercier, S. Sioncke, A. Delabie, W. E. Wang, M. Caymax, M. Meuris, and M. Heyns, Appl. Phys. Lett. **93**, 183504 (2008).